Monte Carlo simulation of x-ray emission by kilovolt electron bombardment

E. Acosta

Facultad de Matemática, Astronomía y Física, Universidad Nacional de Córdoba, Medina Allende y Haya de la Torre, 5000 Córdoba, Argentina

X. Llovet

Serveis Científico-Tècnics, Universitat de Barcelona, Lluís Solé i Sabarís, 1-3, 08028 Barcelona, Spain

E. Coleoni and J. A. Riveros

Facultad de Matemática, Astronomía y Física, Universidad Nacional de Córdoba, Medina Allende y Haya de la Torre, 5000 Córdoba, Argentina

F. Salvat[a]

Facultat de Física (ECM), Universitat de Barcelona, Societat Catalana de Física (IEC), Diagonal 647, 08028 Barcelona, Spain

A physical model for the simulation of x-ray emission spectra from samples irradiated with kilovolt electron beams is proposed. Inner shell ionization by electron impact is described by means of total cross sections evaluated from an optical-data model. A double differential cross section is proposed for bremsstrahlung emission, which reproduces the radiative stopping powers derived from the partial wave calculations of Kissel, Quarles and Pratt [At. Data Nucl. Data Tables **28**, 381 (1983)]. These ionization and radiative cross sections have been introduced into a general-purpose Monte Carlo code, which performs simulation of coupled electron and photon transport for arbitrary materials. To improve the efficiency of the simulation, interaction forcing, a variance reduction technique, has been applied for both ionizing collisions and radiative events. The reliability of simulated x-ray spectra is analyzed by comparing simulation results with electron probe measurements. © *1998 American Institute of Physics.* [S0021-8979(98)01511-4]

I. INTRODUCTION

Theoretical methods to compute accurate x-ray spectra emitted from targets bombarded with kV electrons are required for quantification in electron probe microanalysis (EPMA). These computation methods are useful for spectral background subtraction, specially in the low energy region, and for the development of procedures for quantitative analysis of thin films, small particles and rough surfaces. Calculated spectra are also useful in establishing the minimum detection limits for a specific sample. Last, but not least, reliable theoretical calculations help us to get a comprehensive understanding of the x-ray generation in the target, which is essential for the proper interpretation of measured data.

Monte Carlo simulation has proven to be the most suitable theoretical tool for the computation of x-ray spectra; it can incorporate realistic interaction cross sections and can be applied to complex geometries. Moreover, it allows us to keep track of the evolution of all secondary particles (and their descendants) generated by primary electrons. The main limitation of the Monte Carlo method arises from its random nature; the scored quantities are affected by statistical uncertainties, which may be intolerably large, especially when studying quantities associated with events that very seldom occur. Alternatively, x-ray spectra can also be computed from the numerical solution of the transport equation.[1] However, this kind of solution is only possible for relatively simple interaction models and planar geometries.

In EPMA, Monte Carlo calculations have been mainly used to determine the ionization-depth distribution function $\Phi(\rho z)$ (see, e.g., Refs. 2 and 3). Simulations of the continuous component of x-ray spectra have been carried out by Statham[4] and Heckel and Jugelt,[5] and more recently by Ding *et al.*[6] Similar Monte Carlo simulations have been reported by Araki *et al.*,[7] who included characteristic lines. Gauvin *et al.*[8] have used Monte Carlo simulation results to derive calibration curves for quantitative analysis of particulate matter. In these cases, only the transport of electrons was considered. X-ray absorption and secondary x-ray fluorescence were taken into account by simply assuming exponential attenuation inside the sample. This procedure is only approximate and, moreover, it is difficult to generalize to complex geometries (e.g., samples with inclusions and particulate materials.)[8] This difficulty is overcome here by simulating the transport of both electrons and photons, in such a way that complex geometries can be handled easily and accurately with the aid of available geometry packages.

The reliability of simulated x-ray spectra depends mainly on the accuracy of the adopted interaction cross sections. As x rays are mainly originated by electron impact ionization of inner shells and by bremsstrahlung emission, the differential cross sections (DCS) used to simulate these processes should be the most accurate available. This is not the case for most of the calculations of ionization distribu-

[a]Author to whom correspondence should be addressed; electronic-mail: cesc@ecm.ub.es

tions and x-ray emission for EPMA quantification, where oversimplified approximations are commonly used. Thus, for inner shell ionization, the usual practice is to use either empirical formulas based on the asymptotic limit of the Bethe theory (see e.g., Ref. 9) or the semiclassical approximation proposed by Gryzinski.[10] The first of these formulas are valid only for electron energies well above the ionization threshold (which is not always the case in EPMA), whereas the theoretical foundation of Gryzinski's cross section is questionable for all energies. In the case of bremsstrahlung emission, the common practice is to use a parameterization of the DCS obtained from Sommerfeld's theory[11] due to Kirkpatrick and Wiedmann[12] and Statham.[4] It will be shown below that this parameterization differs very significantly from the more accurate partial wave calculation results tabulated by Kissel *et al.*[13]

The aim of the present article is to describe a more accurate, and still computationally simple, theoretical model for the simulation of x-ray spectra. The model involves improved DCSs for inner shell ionization and bremsstrahlung emission. These DCSs have been implemented on a Monte Carlo program that generates x-ray spectra for homogeneous (or multilayered) samples with arbitrary composition. This program is largely based on the code system PENELOPE,[14] which has been shown to provide a reliable description of electron transport in the energy range of interest in EPMA.[15]

In Sec. II we give a brief overview of the structure of PENELOPE and the underlying physical interaction models. The generation of x-rays is discussed in Sec. III, where we describe the cross sections for electron impact ionization and bremsstrahlung emission and their implementation in the simulation code. In Sec. IV we briefly describe the experimental setup and the reduction of measured x-ray spectra to an absolute scale. Simulation results are compared with measured spectra in Sec. V.

II. THE PHYSICS OF *PENELOPE*

PENELOPE (an acronym that stands for ''PENetration and Energy LOss of Positrons and Electrons'') is a general-purpose subroutine package for the simulation of coupled electron-photon transport in matter.[14] It generates electron-photon showers in homogeneous media, of arbitrary composition, for a wide energy range, from about 1 keV up to about 1 GeV. It also includes a geometry package for simulation of complex geometries consisting of homogeneous bodies limited by quadric surfaces. The complete code system (FORTRAN source files and data base) is available from the Nuclear Energy Agency (NEA) data bank.[16]

The cross sections implemented in PENELOPE and the simulation algorithm (i.e., the set of rules to generate random electron tracks from a given scattering model) have been described in detail elsewhere (see Refs. 14 and 17 and references therein). For the sake of completeness, we summarize here the major features of the simulation algorithm.

A. Electron transport

Elastic scattering of electrons is simulated using a combination of the Wentzel (screened Rutherford) DCS and a fixed-angle scattering process. The analytical DCS contains three parameters that are determined in such a way that the mean free path between collisions and the mean and the variance of the angular deflection in each elastic collision are identical with the values obtained with a realistic numerical DCS. The model is thus completely determined by the values of the mean free path and the first and second transport mean free paths, which have been calculated for all elements using a partial wave method with the Dirac–Hartree–Fock–Slater field, corrected for exchange effects.[18]

Inelastic collisions are described in terms of analytical DCSs[19] based on a simple generalized oscillator strength (GOS) model proposed by Liljequist.[20] In this model the ionization of each atomic electron shell is described by a single oscillator, whose ''resonance energy'' is calculated in such a way that the mean excitation energy I tabulated by Berger and Seltzer[21] is exactly reproduced. This model yields stopping powers that coincide with the values recommended by Berger and Seltzer for energies above 10 keV, and is expected to remain accurate for much smaller energies, down to a few hundred eV. Radiative events are described by means of an empirically modified Bethe-Heitler DCS (see Sec. III B below).

The simulation of electron tracks is performed on the basis of a mixed procedure. Individual hard elastic, inelastic and radiative events (i.e., interaction with polar scattering angle θ or energy loss W larger than preselected, small cutoff values θ_c and W_c) are simulated in a detailed way, that is, by random sampling from the corresponding DCS. Soft events (i.e., interactions with θ or W less than the cutoff values) have a mild influence on the track evolution, which can be accurately described by means of simple multiple scattering theories. The effect of the (usually many) soft interactions that occur between a pair of consecutive hard events is described as a single artificial event in which the particle is deflected and loses energy according to probability distribution functions that are dictated by the multiple scattering theory (''condensed'' simulation). Between each pair of consecutive (hard or artificial) events the particle travels freely with a well-defined energy. The angle cutoff θ_c is automatically adjusted by the program in such a way that the average deflection in each path segment (between a pair of consecutive hard elastic events) is nearly independent of the electron energy; the energy loss cutoff W_c is directly set by the user. The practical advantage of mixed simulation is that the calculation of the effect of soft events is largely simplified. As the simulation of individual soft events takes up a considerable fraction of the computer time, mixed simulation is normally much faster than detailed simulation, and equally accurate. The mixed algorithm implemented in PENELOPE has been formulated in such a way that it provides a consistent description of electron tracks in the vicinity of interfaces (a point that requires special care when using condensed algorithms, see, e.g., Ref. 22).

B. Photon transport

The considered photon interactions are coherent (Rayleigh) scattering, incoherent (Compton) scattering and photoelectric absorption. The cross sections implemented in

PENELOPE are given by simple analytical formulas, with parameters determined from fits to updated interaction data from different sources, mainly Cullen *et al.*[23] and Berger and Hubbell.[24] All random variables are generated by using purely analytical expressions, so that the structure of the simulation code is very simple.

The DCS for coherent scattering is the Rayleigh formula, with the atomic form factor given by a simple rational expression with parameters determined from a fit to the numerical form factors tabulated by Hubbell *et al.*[25] Compton scattering is simulated by means of the relativistic impulse approximation,[26] which accounts for Doppler broadening and binding effects. It is worth noting that the impulse approximation describes Compton interactions with bound electrons, which may cause inner shell ionization and subsequent characteristic x-ray emission. This x-ray generation mechanism is normally disregarded when the simpler DCS obtained from the Waller-Hartree approximation (Klein-Nishina DCS multiplied by the incoherent scattering function)[25] is used to describe Compton events. Photoelectric cross sections are obtained by interpolation in a table generated with the XCOM program of Berger and Hubbell.[24]

III. GENERATION OF X-RAY SPECTRA

In the case of electrons, the simulation algorithm adopted in PENELOPE was devised to provide an accurate description of the penetration and slowing down of these particles and, for the sake of simplicity, the description of certain interactions that occur with exceedingly small probability was oversimplified. Thus, the generation of characteristic x-rays by direct electron impact was disregarded, since the overwhelming majority of inelastic collisions involve electrons in the outer, weakly bound shells of the target atoms. Also, bremsstrahlung emission was described by means of a high energy approximation that gives the correct radiative stopping power for all energies, but the ''intrinsic'' angular distribution of the generated photons (relative to the direction of the emitting electron) becomes inadequate when the electron energy is less than ~1 MeV. Again, this approximation was fully justified since radiative losses represent only a very small fraction of the stopping power of electrons with these energies. For our present purposes, this is unfortunate since the spectrum is built by detecting photons generated precisely through these two processes.

We have previously shown that PENELOPE provides a good description of the transport of kV electrons[15] and, therefore, the generated electron tracks can be considered as numerical replicas of actual tracks. Owing to this fact, we can evaluate the space distribution of emitted characteristic x-rays without altering the simulation routines. The only information we need is the total ionization cross section of the shell of interest as a function of the electron energy, which determines the probability of ionization along each segment of an electron track generated by PENELOPE.[3] For the simulation of radiative events, the core of the simulation package had to be modified as described below.

A. Characteristic x-ray emission

Inelastic collisions of electrons of energy E can be described in terms of the energy loss W and the ''recoil energy'' Q defined by

$$Q \equiv \frac{q^2}{2m}, \tag{1}$$

where q is the momentum transfer and m is the electron mass. The recoil energy is related to the polar scattering angle θ by the kinematic formula

$$Q = 2E - W - 2\sqrt{E(E-W)}\cos\theta. \tag{2}$$

The DCS for ionization of bound shells by electron impact, computed within the first Born approximation, can be written as[27]

$$\frac{d^2\sigma}{dQ\,dW} = \frac{\pi e^4}{E} \frac{1}{WQ} \frac{df(Q,W)}{dW}, \tag{3}$$

where $df(Q,W)/dW$ is the generalized oscillator strength (GOS) density per unit energy transfer W for ionization of that shell. Here we approximate the GOS according to the optical model proposed by Mayol and Salvat,[28]

$$\frac{df(Q,W)}{dW} \simeq \frac{mc}{2\pi^2 e^2 \hbar^2} \int \sigma_{ph}(W')$$
$$\times [\delta(W-W')\Theta(W'-Q)$$
$$+ \delta(W-Q)\Theta(Q-W')]dW', \tag{4}$$

where e is the electron charge, c is the velocity of light in vacuum and $\sigma_{ph}(W')$ is the photoelectric cross section for ionization of the considered shell by photons of energy W' (which is proportional to the optical oscillator strength). The term $\delta(x)$ represents the Dirac δ distribution and $\Theta(x)$ ($=1$ if $x>0$, $=0$ otherwise) is the Heaviside step function. Exchange effects are accounted for by means of a modified Ochkur correction (see Ref. 28), which leads to the formula

$$\frac{d^2\sigma}{dQ\,dW} = \frac{\pi e^4}{E} \frac{1}{WQ} \frac{mc}{2\pi^2 e^2 \hbar^2} \int \sigma_{ph}(W')$$
$$\times [\delta(W-W')\Theta(W'-Q)$$
$$+ \delta(W-Q)\Theta(Q-W')] C_{ex} dW' \tag{5}$$

with

$$C_{ex} = 1 - \frac{Q}{E+W'-W} + \left(\frac{Q}{E+W'-W}\right)^2. \tag{6}$$

The total ionization cross section is given by

$$\sigma_i(E) = \int_{E_i}^{E/2} dW \int_{Q_{min}}^{Q_{max}} \frac{d^2\sigma}{dQ\,dW} dQ, \tag{7}$$

where E_i is the ionization energy of the shell and the limits of the integral over Q are given by expression (2) with $\theta=0$ and π. Thus, the ionization cross section is completely determined by the photoelectric cross section. Tables of σ_{ph} for the different shells of all the elements have been calculated by Scofield.[23] For the sake of simplicity, we shall only

J. Appl. Phys., Vol. 83, No. 11, 1 June 1998
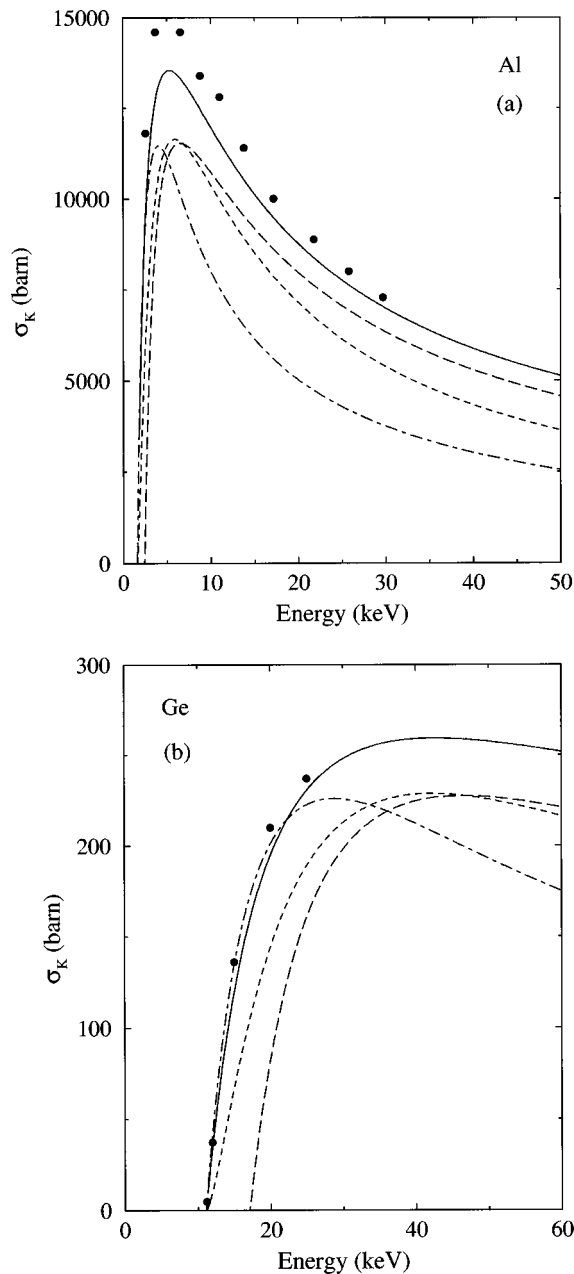
Acosta *et al.* 6041

FIG. 1. Electron impact K-shell ionization cross section for Al (a) and Ge (b). Symbols represent experimental data from the compilation in Ref. 30. The continuous curves are results from the optical data model described in Sec. III A. The other curves represent cross sections obtained from the analytical formulas of Gryzinski (dashed), Worthington-Tomlin (dotdashed) and Bethe-Powell (long-dashed). $(1 \text{ mb} = 10^{-27} \text{ cm}^2)$.

consider the ionization of K shells. In this case, a hydrogenic model[28] provides a simple and sufficiently accurate analytical approximation for σ_{ph}.

K-shell total ionization cross sections of aluminium and germanium, calculated from Eq. (7), are compared with experimental data in Fig. 1. This figure also displays cross sections obtained from the following analytical approximations, of common use in EPMA studies: The Gryzinski[10] cross section

$$\sigma_K^2 E_K^2 = \pi e^4 Z_K g(U_K), \qquad (8)$$

where

$$g(U_K) = \frac{1}{U_K}\left[\frac{U_K-1}{U_K+1}\right]^{3/2}\left[1+\frac{2}{3}\left(1-\frac{1}{2U_K}\right)\right.$$

$$\left. \times \ln[2.7+(U_K-1)^{1/2}]\right], \qquad (9)$$

the Worthington-Tomlin formula[29]

$$\sigma_K^2 E_K^2 = \pi e^4 Z_K a_K \frac{\ln(U_K)}{U_K} \ln\left[\frac{4U_K}{1.65+2.35 \exp(1-U_K)}\right] \qquad (10)$$

with $a_K = 0.35$, and the Bethe-Powell formula[9]

$$\sigma_K^2 E_K^2 = \frac{\pi e^4 Z_K b_K}{U_K} \ln(c_K U_K) \qquad (11)$$

with $b_K = 0.9$ and $c_K = 0.65$, where E_K denotes the ionization energy of the K shell, $U_K \equiv E/E_K$ is the over voltage and Z_K is the number of electrons in the shell. Owing to the scarcity of absolute measurement results,[30] a mere comparison with experimental data does not provide definite conclusions about the accuracy of the various formulas. For the two elements in Fig. 1, the present optical-data model predicts an energy dependence of σ_K in reasonably good agreement with experiment. This is also the case for other elements that have been analyzed, using experimental data collected in Ref. 30. As the physical contents of the optical-data model are sound, we shall assume that it yields the best estimates for σ_K. Very likely, it does provide a better description of the dependence of σ_K on the atomic number Z than the analytical formulas (8)-(11). In this respect, it is worth noting that these analytical formulas depend on the atomic number only through the ionization energy E_K (apart from a change in the scales, the corresponding curves in Fig. 1 are identical for both elements). Judging by the different relative positions of the optical-data model curves for the two elements, we may expect that the true dependence of σ_K on Z is somewhat more involved.

PENELOPE generates electron tracks as a series of ''free flights'' between consecutive (hard and artificial) interactions. Along each free flight, the energy E of the electron is assumed to stay constant. To simulate the generation of characteristic x-rays, which result from vacancies produced in a K shell, we proceed as follows. For each free flight, we calculate the probability that an ionization has been produced in the considered shell, which is given by

$$P_{ion} = s \, \mathcal{N} \, \sigma_i(E), \qquad (12)$$

where s is the length of the free flight and $\mathcal{N}$ is the density of atoms of the considered (ionized) element per unit volume. After computing the ionization probability, we sample a random value ξ uniformly in (0,1) and consider that the interaction is effective only when $\xi < P_{ion}$. When an ionization occurs, its position is sampled uniformly along the free flight. As the probability of ionization in a free flight is much less than unity, this procedure gives the correct average number of ionizations per unit path length.

Excited ions relax to their ground state by migration of the initial vacancy to outer electron shells, which proceeds through emission of fluorescent x rays or Auger electrons

with characteristic energies. Our code, as well as PENELOPE, simulates the emission of characteristic x rays that result from vacancies produced in a K shell. We consider only characteristic photons emitted in the first stage of the de-excitation cascade, i.e., when the initial vacancy in the K shell is filled by an electron from an outer shell. The probability that a radiative de-excitation occurs is obtained from the fluorescence yields tabulated by Fink and Rao.[31] The considered characteristic photons are K_α and K_β, with relative probabilities obtained from the line fractions given by Khan and Karimi.[32] Characteristic x-rays are assumed to be emitted isotropically.

To improve the efficiency of the simulation, we apply interaction forcing, which is also known as the ''method of statistical weights.'' This consists of artificially increasing the probability of ionization along a free flight, say to a value P_{fi}. To compensate for this increase of probability, characteristic x-rays emitted in the forced interaction are given a weight $\omega = P_{ion}/P_{fi}$ less than unity. This manipulation does not alter the computed spectra, but the statistical uncertainties (for a given calculation time) are substantially reduced. In the calculations, we adopt a value of P_{fi} such that, on average, 0.1 forced ionizations occur along each free flight.

B. Bremsstrahlung emission

PENELOPE samples the energy W of the emitted bremsstrahlung photons from a modified Bethe-Heitler (BH) DCS for an exponentially screened Coulomb field, integrated over the angles of scattering and emission. The original Bethe-Heitler DCS[33] provides a simple analytical formula for the energy distribution of the emitted photons, which is well suited for random sampling. However, it is based on the Born approximation and, therefore, valid only for high energy electrons.[34] Salvat and Fernández-Varea[19] introduced an empirical correction term that extends its validity to lower energies. The modified energy-loss Bethe-Heitler DCS for an element of atomic number Z is given by

$$\frac{d\sigma_{BH}}{dW} = C_{BH}\left(\varphi_1(\epsilon) + \frac{1}{\epsilon}\varphi_2(\epsilon)\right), \qquad (13)$$

where ϵ is the reduced energy of the emitted photon

$$\epsilon \equiv \frac{W}{E + mc^2}. \qquad (14)$$

The quantities $\varphi_1(\epsilon)$ and $\varphi_2(\epsilon)$ are functions of ϵ and Z given by simple analytical expressions (see Ref. 19). The ''normalization'' constant C_{BH} is determined in such a way that the DCS given by Eq. (13) exactly reproduces the radiative stopping powers for electrons in single element materials tabulated by Berger and Seltzer,[21] which were derived from the partial wave calculations of Kissel *et al.*[13] Thus the DCS (13) provides a fairly good approximation for the electron mean free path between radiative events and for the distribution of energy losses in those events. However, the angular distribution of the emitted photons must be obtained by other means.
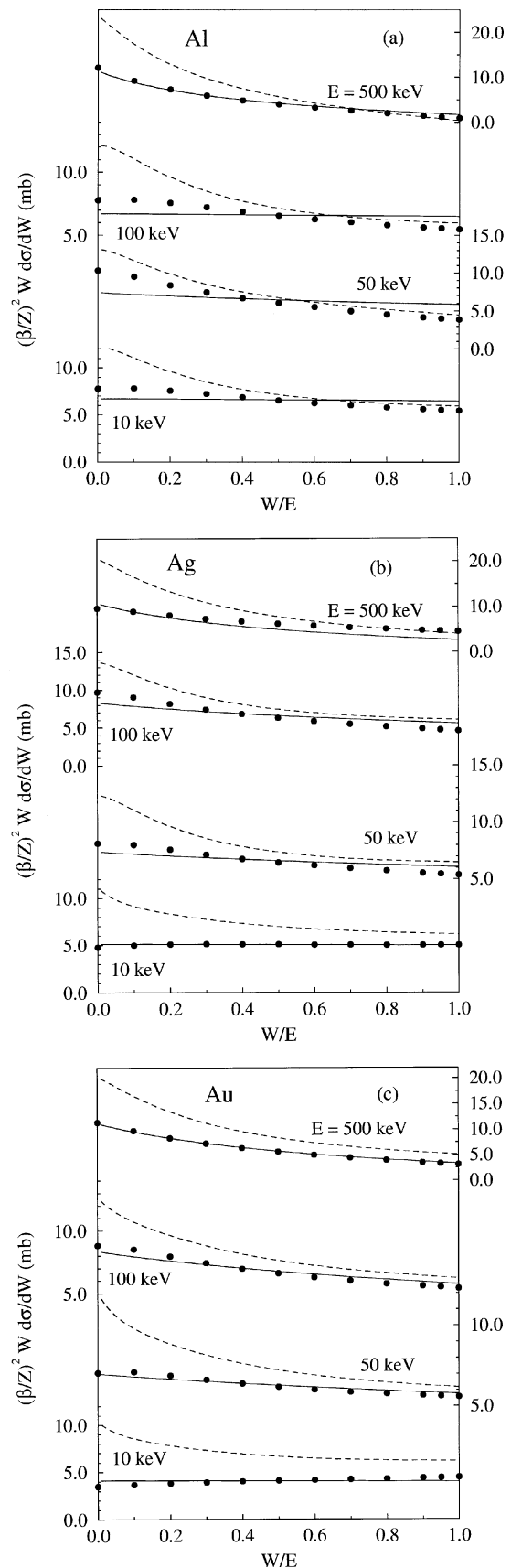

FIG. 2. Reduced energy-loss DCSs, i.e., DDCS integrated over angles and multiplied by $(\beta/Z)^2 W$, for bremsstrahlung emission by electrons in Al (a), Ag (b) and Au (c). Dashed curves, Kirkpatrick-Wiedmann-Statham formula, Eq. (17); continuous lines, modified Bethe-Heitler formula, Eq. (13). Dots represent tabulated results of Kissel *et al.* (Ref. 13). Notice that the vertical scale for each energy is the closest to its label.

The direction of the emitted photon, relative to that of the primary electron, is defined by the polar angle θ and the azimuthal angle ϕ. Considering that the atomic field is spherically symmetric, the angular distribution of the emitted photon is independent of ϕ; therefore, the azimuthal scattering angle is distributed uniformly in the interval $(0,2\pi)$. In PENELOPE, the polar angle is sampled from the distribution obtained from the classical dipole approximation (see, e.g., Ref. 35)

$$p_{\text{dipole}}(\cos\theta) = \frac{3}{16\pi}\left[1 + \left(\frac{\cos\theta - \beta}{1 - \beta\cos\theta}\right)^2\right]\frac{1 - \beta^2}{(1 - \beta\cos\theta)^2},$$

(15)

where $\beta = v/c$ is the velocity of the electron in units of the speed of light c ($\beta^2 = 1 - \gamma^{-2}$). This angular distribution is reasonably accurate for energies above ~ 1 MeV, but becomes incorrect at lower energies.

The double differential cross section (DDCS), differential in the photon energy and direction of emission, used in PENELOPE, can be written as

$$\frac{d^2\sigma_{\text{BHd}}}{dWd\Omega} = C_{\text{BH}}\left(\varphi_1(\epsilon) + \frac{1}{\epsilon}\varphi_2(\epsilon)\right)\frac{1}{2\pi}p_{\text{dipole}}(\cos\theta).$$

(16)

Sempau *et al.*[14] have shown that PENELOPE gives a fairly accurate description of bremsstrahlung spectra generated by kilovolt electrons in thick samples, in spite of the limitations of the intrinsic angular distribution (15). The reason for this is that, in the case of bulk targets, the electron trajectories are rapidly randomized by elastic scattering and the angular distribution of photons emerging through the surface is practically insensitive to the intrinsic angular distribution. However, for thin films and small particles the effect of the angular dependence of the cross section may be important and a more accurate intrinsic distribution should be used.

Kissel *et al.*[13] computed bremsstrahlung DCSs for energies between 1 and 500 keV by partial wave methods. Their results are the most accurate data available for the energy range of interest in EPMA, but they consist of large tables difficult to handle within a simulation code. Previously, Kirkpatrick and Wiedmann[12] proposed an analytical DCS based on the Sommerfeld[11] theory, which was subsequently modified by Statham[4] to get a closer fit to the theoretical

values for small energies. This is the most commonly used model in Monte Carlo simulations for EPMA. However, Sommerfeld's theory is known to be in error for kilovolt electrons, as pointed out by e.g., Chapman *et al.*[36] Surprisingly, we have found that the Kirkpatrick-Wiedmann-Statham (KWS) formula predicts angular distributions in fairly good agreement with the calculations of Kissel *et al.*

The KWS double differential cross section (DDCS) for bremsstrahlung emission is given by the following general expression:

$$\frac{d^2\sigma_{\text{KWS}}}{dWd\Omega} = \frac{\sigma_x(1 - \cos^2\theta) + \sigma_y(1 + \cos^2\theta)}{(1 - \beta\cos\theta)^2},$$

(17)

where σ_x and σ_y are parameters that depend on the electron incident energy E, the emitted photon energy W and the atomic number Z of the target. Kirkpatrick and Wiedmann[12] obtained analytical approximations for the parameters σ_x and σ_y and Statham[4] modified the expressions of σ_x and σ_y to produce a better fit to the theoretical data at small electron energies. The final analytical formulas for σ_x and σ_y can be found in Ref. 6.

Energy-loss bremsstrahlung DCSs obtained from the modified Bethe-Heitler formula (13) and from the KWS formula (17), integrated over angles, are compared with Kissel's *et al.*'s data in Fig. 2 (the area below the curves is proportional to the radiative stopping power). Notice that, for low energy electrons, the BH formula gives an energy-loss DCS proportional to W^{-1}, in accordance with the numerical results. Moreover, owing to the definition of the normalization constant C_{BH} in Eq. (13), the areas below the modified BH curves and below the data of Kissel *et al.* are equal. On the other hand, the KWS formula clearly overestimates the energy-loss DCS, and the radiative stopping power, in the considered energy range.

In order to get a more accurate formula for the DDCS than the approximations given by Eqs. (16) and (17), we shall tentatively combine the modified Bethe-Heitler DCS, Eq. (13), with the angular distribution derived from the KWS DCS

$$p_{\text{KWS}}(\cos\theta) = N_\theta\frac{\sigma_x(1 - \cos^2\theta) + \sigma_y(1 + \cos^2\theta)}{(1 - \beta\cos\theta)^2},$$

(18)

where

$$N_\theta = \frac{\beta^3(1 - \beta^2)}{2\{2\beta\sigma_y - 2\beta(1 - \beta^2)\sigma_x + [\log(1 - \beta) - \log(1 + \beta)](1 - \beta^2)(\sigma_y - \sigma_x)\}}$$

(19)

is a normalization constant such that

$$\int_{-1}^{1} p_{\text{KWS}}(\cos\theta)d(\cos\theta) = 1.$$

(20)

The proposed DDCS reads

$$\frac{d^2\sigma_{\text{BK}}}{dWd\Omega} = C_{\text{BH}}\left(\varphi_1(\epsilon) + \frac{1}{\epsilon}\varphi_2(\epsilon)\right)\frac{1}{2\pi}p_{\text{KWS}}(\cos\theta).$$

(21)

As shown in Fig. 3, this analytical formula predicts values that are in closer agreement with the numerical cross sections tabulated by Kissel *et al.*[13] In the present simulations, bremsstrahlung emission is simulated according to this DDCS.
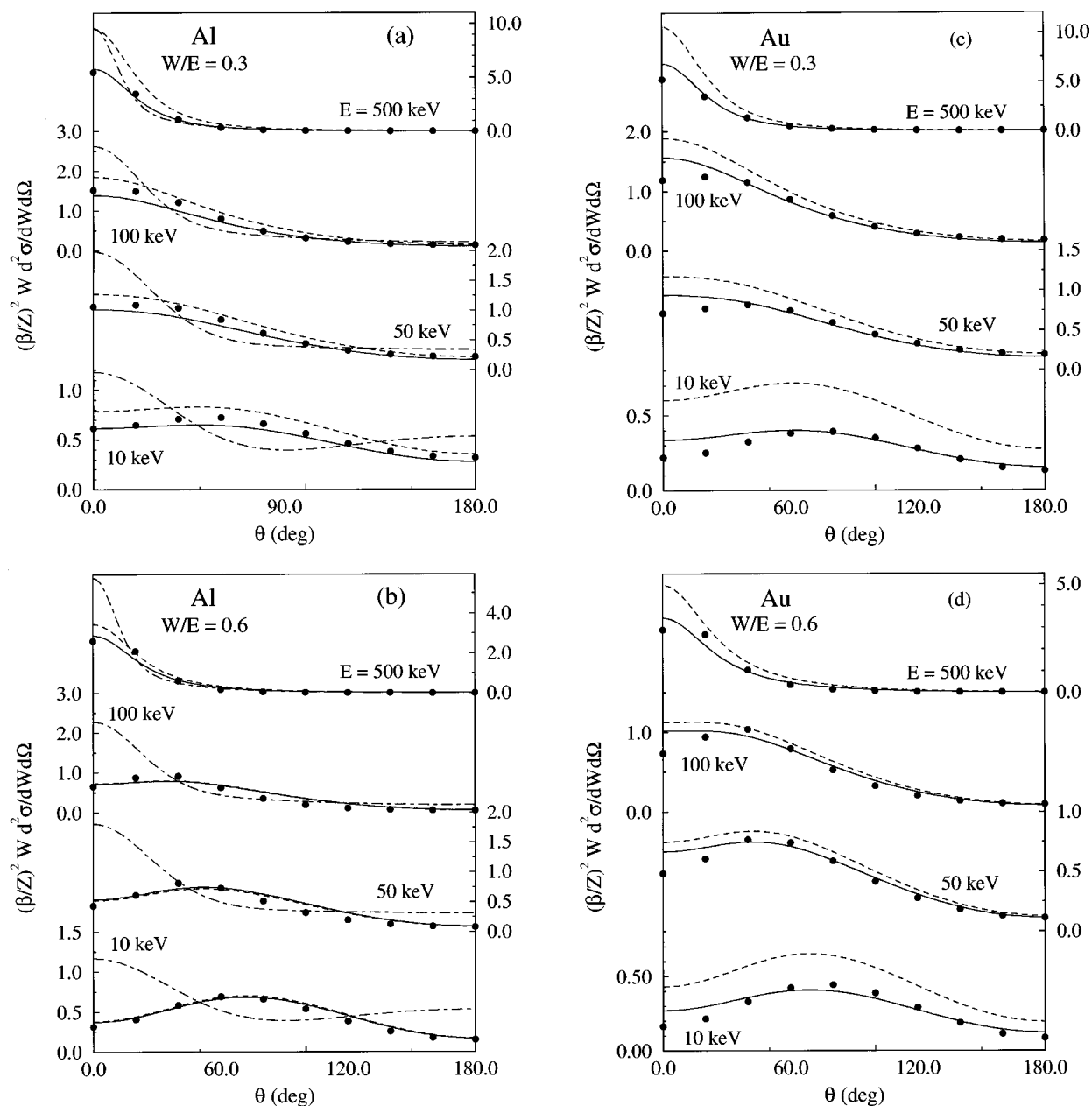
FIG. 3. Electron bremsstrahlung reduced DDCSs for different elements and photon-to-electron energy ratios W/E: Al, $W/E = 0.3$ (a); Al, $W/E = 0.6$ (b); Au, $W/E = 0.3$ (c) and Au, $W/E = 0.6$ (d). Dot-dashed curves (only for Al), modified Bethe-Heitler DCS model with dipole angular distribution, Eq. (16); dashed curves, Kirkpatrick-Wiedmann-Statham DDCS, Eq. (17); solid curves, modified Bethe-Heitler DCS with KWS angular distribution, Eq. (21). Dots represent numerical data calculated by Kissel *et al.* (see Ref. 13). The vertical scale for each energy is the closest to its label.

That is, the mean free path and energy loss distributions are the same as in the original PENELOPE code, but the initial direction of the emitted photon is generated according to the intrinsic distribution (18). The algorithm for random sampling of $\cos\theta$ is described in Appendix A. Changing to this improved angular distribution required only a minor modification of the original PENELOPE code.

Since bremsstrahlung emission by keV electrons is a low probability process, we again apply interaction forcing to reduce the statistical uncertainties. In this case, we multiply the bremsstrahlung inverse mean free path by a factor $P_{fr} > 1$ and, to compensate for this, bremsstrahlung photons, and their descendents, are assigned a weight $\omega = 1/P_{fr}$. The factor P_{fr} is chosen in such a way that the reduced inverse

mean free path is of the order of 1/5 of the electron range. This assures that a mean number of five bremsstrahlung photons per primary electron are produced.

A steering program has been written to simulate EPMA measurements using the PENELOPE routines modified as described above. The program generates energy distributions of x rays emitted from the specimen, per incident electron and per unit solid angle, in the direction of the x ray detector. To calculate each theoretical spectrum we have simulated about 500 000 primary electron tracks. The statistical uncertainties of the results in the significant portions of the spectrum (characteristic peaks and background at intermediate energies) are then less than 5%.

IV. EXPERIMENTAL METHOD: ABSOLUTE SPECTRA

Thick targets, pure elements and compounds have been irradiated with 20 and 30 kV electron beams at normal incidence using an electron microprobe CAMECA SX-50. Spectra of emerging x rays have been obtained by using a PGT IMIX energy dispersive spectrometer, located in a direction forming an angle of 40° with the sample surface. The spectrometer is a Si(Li) detector. According to the manufacturer's specifications, the Si(Li) crystal is 3 mm thick and has an active area of approximately 12.5 mm^2. The detector has a 7-μm-thick beryllium window and a contact gold layer 0.02 μm thick. The thickness of the Si dead layer is 0.1 μm.

The emerging photon beam has been collimated with a diaphragm (300 μm in diameter) placed in front of the beryllium window, at 53 mm from the target. This avoids spurious x-ray peaks caused by electrons backscattered onto the pole piece of the final lens of the microscope column and other objects near the specimen. Probe currents have been measured with a Faraday cup placed on the sample holder, and have been chosen so as to yield a counting rate below 1000 counts per second, thus minimizing pulse pileup effects. Typical acquisition times were 3000-4000 s.

Acquired x-ray spectra have been converted to absolute intensity units, i.e., number of photons emitted per unit energy interval and unit solid angle per incident (bombarding) electron. It is worth pointing out that measurements in absolute units serve as the most stringent test of the physical parameters used in the simulation algorithm, although they may contain systematic uncertainties. The conversion of the acquired spectra to absolute intensity is made by using the equation

$$N(E) = \frac{N_{\text{ch}}}{N_0 \epsilon(E) \Delta \Omega \Delta E}, \tag{22}$$

where N_{ch} is the number of counts in a particular photon energy channel, N_0 is the total number of incident electrons, $\Delta \Omega$ is the solid angle subtended by the x-ray detector, ΔE is the width of the energy channel and $\epsilon(E)$ is the detector efficiency, which is a function of the photon energy.

The number of incident electrons N_0 has been evaluated by multiplying the target current I_0 by the acquisition time t. We recall that the electron microprobe has a built-in continuous beam current monitoring and feedback system, which stabilizes the beam current to 0.3%. The calculated number of incident electrons is estimated to have less than 2% uncertainty. The width of the photon energy channel ΔE of the spectra is given by the computer of the PGT IMIX system. The high energy part of the x-ray spectrum (bremsstrahlung tip) has been used to verify the accelerating potential values. The solid angle $\Delta \Omega$ has been computed as A/d^2, where A is the area of the entrance aperture of the collimator, and d is the distance between the sample and the collimator. Using the values for A and d given by the manufacturer, the uncertainty in $\Delta \Omega$ is estimated to be less than 2%.

The efficiency of a Si(Li) x-ray detector is essentially unity over a wide photon energy interval ($\sim$3-15 keV). It takes lower values at low photon energies, due to absorption in the different inactive layers in front of the intrinsic zone,

and at high energies, due to partial transmission through the intrinsic zone. In general, the efficiency can be evaluated by using radioactive sources of known activity,[37] well-calibrated fluorescence sources or synchrotron radiation,[38] and/or theoretical methods.[39] As a first approximation, $\epsilon(E)$ can be computed by assuming exponential attenuation of the photon beam in the inactive layers and in the intrinsic zone. However, this approach may be in serious error due to the following reasons. First, the different layers are generally nonuniform (see, e.g., Ref. 40) and their average thicknesses are poorly known. Secondly, absorption of photons with moderately high energy in the inactive layers produces secondary radiation (photoelectrons and x rays) that may yet reach the active zone. Recently, Lepy *et al.*[41] have shown that the so-called silicon ''dead layer'' acts as a partially active layer, the corresponding events being recorded in the peak tail. Finally, uncertainties of adopted attenuation coefficients also affect the estimated efficiency.

Assuming, for a moment, that simulated spectra are reliable (see below), one can use them to analyze the consistency of calculated efficiencies. We have tentatively evaluated the efficiency $\epsilon(E)$ by considering purely exponential attenuation and using the detector layer thicknesses given by the manufacturer. Direct comparison of simulated spectra with experiments confirms that the efficiency is close to unity for photons with energy in the interval from $\sim$3 up to $\sim$15 keV, as predicted by the simple calculation. However, this calculation underestimates $\epsilon(E)$ at lower energies, and overestimates it at higher energies, justifying the presence of the aforesaid sources of error. To get at least a rough estimate of $\epsilon(E)$ for the complete energy range of interest, we have computed it by considering absorption only in the most significant passive layer, i.e., the Be window, and using an effective value for the crystal thickness (1.5 mm), as suggested by the work of Paterson *et al.*[42] With this method one gets efficiencies that are accurate to within $\sim$5% for energies between 3 and 15 keV and ''plausible'' outside this range. Therefore, comparison of simulated and measured spectra is meaningful for $E = 3$-15 keV and only indicative for lower and higher energies.

Finally, uncertainties from counting statistics range typically from 3 to 6% in the continuous component of the spectra, and 1%-2% in the characteristic peaks. Other sources of uncertainty, such as errors in the estimate of the take-off angle and target uniformity, are considered to be negligible. The various error contributions discussed above lead to an overall uncertainty of 5%-7% for the experimental absolute spectra.

V. COMPARISON OF SIMULATED AND MEASURED SPECTRA

Energy distributions of x-rays emitted from the specimen in directions close to that of the detector have been simulated using the code described above. To account for the response of the detector, Monte Carlo spectra have been convoluted with a Gaussian distribution with an energy-dependent full width at half maximum (FWHM). The dependence of the FWHM on incident photon energy has been estimated by measuring x-ray spectra for different pure

specimens, whose characteristic x-ray energies span the region between 1 and 10 keV. Simulated spectra have been normalized to one incident electron to make them directly comparable to measured absolute spectra.

Simulated and experimental spectra, at incident electron energies of 20 keV, for Cu and Ag metallic targets as well as for a Fe-Cr-Ni alloy (standard reference material 479a, certified by the National Bureau of Standards (NBS), with weight concentrations of 71%, 18.1% and 10.9%, respectively), are compared in Fig. 4. It can be observed that the agreement is, in general, satisfactory in the "meaningful" region between 3 and 15 keV. The calculation also describes the continuous component of the spectra accurately, even in regions where uncertainties in $\epsilon(E)$ may be somewhat larger. In the case of Ag, the peak at 3 keV corresponds to L_α x-rays that are not simulated by the present version of the code. The code, however, does give a realistic description of the spectral background below this peak, thus providing valuable information for background subtraction in quantitative analysis.

When comparing simulations with experimental data, we must recall that there are various detection artifacts, such as incomplete charge collection, pulse pileup and sum peaks,[43] which cannot be totally avoided, and whose effects are not taken into account in the simulations. These effects, combined with the uncertainty of the adopted ionization cross sections, originate small discrepancies in the characteristic peaks. It should also be noted that, due to incomplete charge collection, the low energy end of the spectrum accumulates degraded counts from all higher energy x rays, especially in the 0-3 keV region.[43]

Figure 5 displays spectra obtained at incident electron energies of 30 keV from a Cu target and the Fe-Cr-Ni alloy target. Although characteristic peaks again show small discrepancies, duplicating the differences found for 20 keV beams, the agreement between simulation and experiment is again satisfactory. The Cu measured spectrum shows a small (and undesirable) sum peak. In both cases, the simulation is seen to predict the shape of the spectral background accurately in the energy range 3-15 keV, where the uncertainty in $\epsilon(E)$ is small.

Monte Carlo simulation of electron-photon showers can also be used to study secondary fluorescence produced by bremsstrahlung photons. Figure 6 shows a comparison between the complete simulated spectrum from a ZnS target (continuous) and the spectrum simulated for the same target but disregarding ionization produced by electron impact (dashed). It can be observed that, although electron impact ionization has been disconnected, there is an important count rate at the characteristic line energies due to continuum fluorescence. Thus, the present Monte Carlo simulation of electron-photon showers provides a valuable tool to validate theoretical models describing the continuum fluorescence contribution, which is impossible to discriminate experimentally.

It can be concluded that the physical models described here offer a consistent description of x-ray spectra generated by kV electron beams. The differences between simulation and experiment are mostly due to measurement artifacts, and
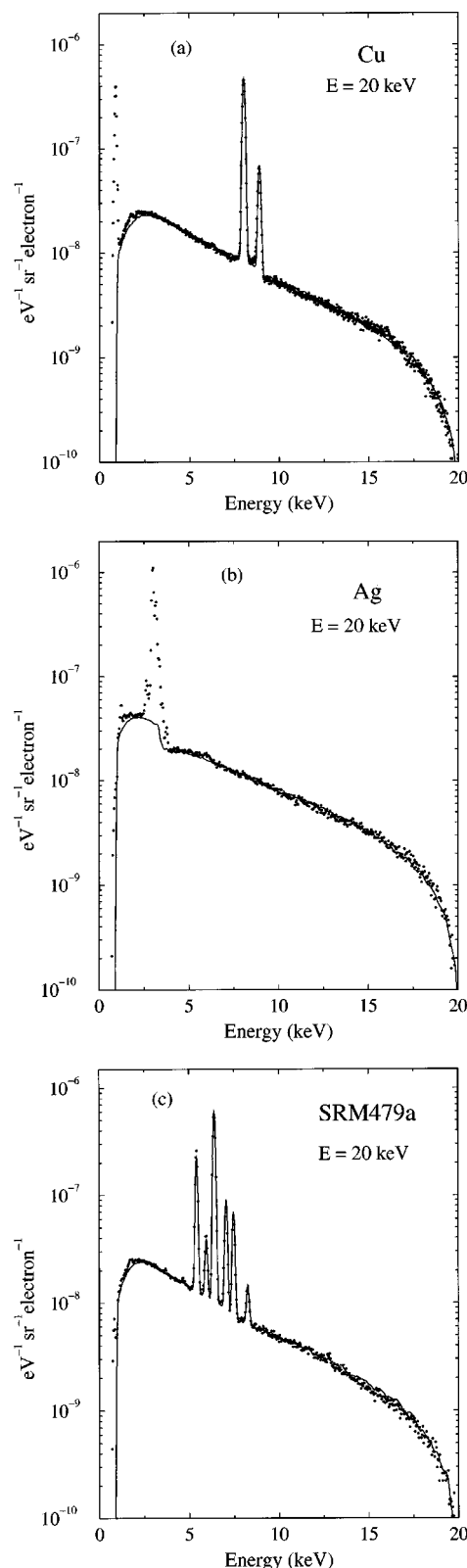

FIG. 4. Simulated (solid line) and experimental (dots) x-ray spectra from copper (a), silver (b) and SRM479a NBS certified standard (c) generated by 20 kV electron beams at normal incidence.

certainly less than those obtained with other models previously proposed. Our simulation algorithm is well suited to compute x-ray spectra from elemental and compound targets, and is a valuable tool for quantitative microanalysis. A study
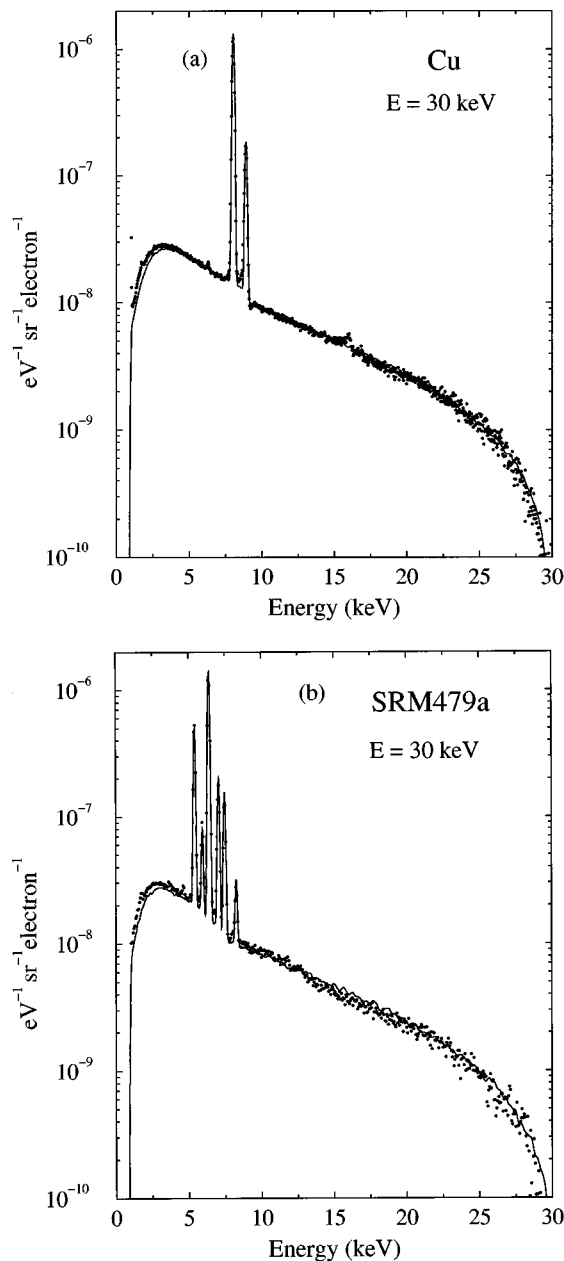
FIG. 5. Simulated (solid line) and experimental (dots) x-ray spectra from copper (a) and SRM479a NBS certified standard (b) generated by 30 kV electron beams at normal incidence.

of x-ray spectra for other geometries of interest in microanalysis (oblique incidence, multilayered targets) will be published elsewhere.[44] In its present form, our computer code can only generate characteristic peaks resulting from K-shell ionization of any element; work to include L-shell ionization is in progress.
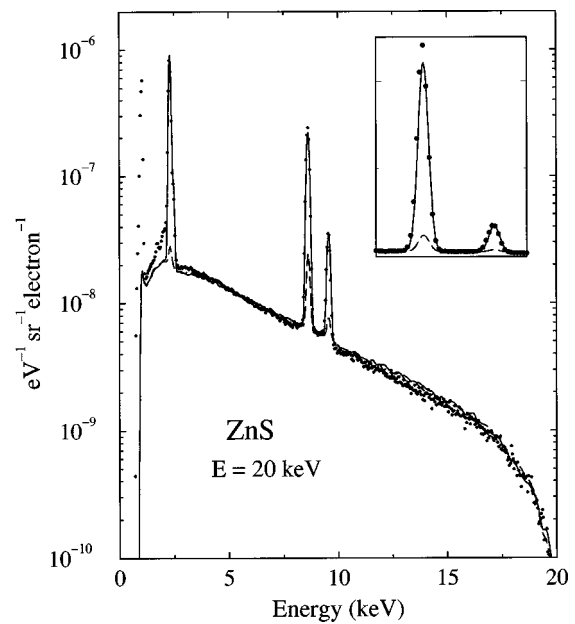
ACKNOWLEDGMENTS

FIG. 6. Measured (dots) and simulated (lines) X-ray spectra from a ZnS target irradiated with a 20 kV electron beam at normal incidence. The continuous spectrum is the result of a complete simulation. The long dashed spectrum is the result of a simulation in which the generation of characteristic x rays by electron impact has been switched off.

APPENDIX A:

In this appendix we describe the algorithm used to sample the initial direction of bremsstrahlung photons from the KWS distribution (18)

$$p_{KWS}(\cos\theta) = N_\theta \frac{\sigma_x(1-\cos^2\theta) + \sigma_y(1+\cos^2\theta)}{(1-\beta\cos\theta)^2}.$$

We first note that this distribution can be cast in the following form

$$p_{KWS}(x) = u_1 p_1(x) + u_2 p_2(x) + u_3 p_3(x), \tag{A1}$$

where $x \equiv \cos\theta$ and

$$p_1(x) = N_1 \frac{1-x^2}{(1-\beta x)^2}, \quad p_2(x) = N_2 \frac{1}{(1-\beta x)^2},$$

$$p_3(x) = N_3 \frac{x^2}{(1-\beta x)^2} \tag{A2}$$

are distributions, normalized to unity, with normalization constants

$$N_1 = \frac{\beta^3}{2[-2\beta + \ln(1+\beta) - \ln(1-\beta)]}, \tag{A3}$$

$$N_2 = \frac{1-\beta^2}{2}, \tag{A4}$$

TABLE I. Efficiency ϵ of the combined composition-rejection algorithm for random sampling from the probability distribution function (PDF) given by Eq. (A1).

W(keV)	Al (Z=13) E(keV)			Ag (Z=47) E(keV)			Au (Z=79) E(keV)		
	10	30	50	10	30	50	10	30	50
1	67	67	68	67	67	68	67	67	68
10	66	66	66	66	66	66	66	66	66
20		65	65		65	65		65	65
40			63			64			64

$$N_3 = \frac{\beta^3(1-\beta^2)}{2\{2\beta - \beta^3 + (1-\beta^2)[\ln(1-\beta) - \ln(1+\beta)]\}}.$$
(A5)

The relative weights in Eq. (A1) are given by

$$u_1 = \frac{N_\theta \sigma_x}{N_1}, \quad u_2 = \frac{N_\theta \sigma_y}{N_2}, \quad u_3 = \frac{N_\theta \sigma_y}{N_3}.$$
(A6)

The distribution $p_2(x)$ can be sampled by using the inverse transform method, which gives the sampling formula

$$x = \frac{2\xi - 1 + \beta}{2\beta\xi + 1 - \beta},$$
(A7)

where ξ is a random number uniformly distributed in the interval (0,1).

The distributions p_1 and p_3 can be rewritten as

$$p_1(x) = \frac{N_1}{N_2} r_1(x) p_2(x), \quad r_1(x) = 1 - x^2,$$
(A8)

$$p_3(x) = \frac{N_3}{N_2} r_3(x) p_2(x), \quad r_3(x) = x^2.$$
(A9)

Since $r_1(x)$ and $r_3(x)$ are smaller than 1, a rejection method can be used to sample x from p_1 and p_3.

The sampling algorithm for the combined distribution (A1) is:

(1) Sample an integer $i(=1,2,3)$ from the point probabilities

$$\pi(1) = \frac{u_1}{\Sigma u_j} = \frac{N_\theta \sigma_x}{N_1}, \quad \pi(2) = \frac{u_2}{\Sigma u_j} = \frac{N_\theta \sigma_y}{N_2},$$

$$\pi(3) = \frac{u_3}{\Sigma u_j} = \frac{N_\theta \sigma_y}{N_3}.$$
(A10)

(2) Sample a value t from $p_2(t)$ using Eq. (A7).
(3) If $i=2$, deliver $x=t$.
(4) If $i=1$, generate a random number ξ.
   (a) If $\xi > r_1(t) = 1 - t^2$, go to step 2.
   (b) Deliver $x=t$.
(5) If $i=3$, generate a random number ξ.
   (a) If $\xi > r_3(t) = t^2$, go to step 2.
   (b) Deliver $x=t$.

As a measure of the effectiveness of the sampling algorithm, we define the efficiency ϵ as the percentage of generated t values that are not rejected (i.e., $100/\epsilon$ is the average number of times that step 2 is executed to generate a single value of x). Efficiencies (obtained after sampling 100 000 x values) for energies of interest in EPMA are given in Table I.

[1] D. B. Brown and J. V. Gilfrich, J. Appl. Phys. **42**, 4044 (1975).
[2] P. Karduck and W. Rehbach, in *Electron Probe Quantitation*, edited by K. F. J. Heinrich and D. E. Newbury (Plenum, New York, 1991), p. 191.
[3] X. Llovet, J. A. Riveros and F. Salvat, Mikrochim. Acta Suppl. **13**, 409 (1996).
[4] P. J. Statham, X-Ray Spectrom. **5**, 154 (1976).
[5] J. Heckel and P. Jugelt, Exp. Tech. Phys. (Berlin) **31**, 493 (1983).
[6] Z. J. Ding, R. Shimizu, and K. Obori, J. Appl. Phys. **76**, 11 (1994).
[7] K. Araki, Y. Kimura, and R. Shimizu, Scanning Microsc. Suppl. **7**, 81 (1993).
[8] R. Gauvin, G. L'Espérance, and S. St.-Laurent, Scanning **14**, 37 (1992).
[9] C. J. Powell, Rev. Mod. Phys. **48**, 33 (1976).
[10] M. Gryzinski, Phys. Rev. **138**, A336 (1965).
[11] A. Sommerfeld, Ann. Phys. (Leipzig) **11**, 257 (1931).
[12] P. Kirkpatrick and L. Wiedmann, Phys. Rev. **67**, 321 (1945).
[13] L. Kissel, C. A. Quarles, and R. H. Pratt, At. Data Nucl. Data Tables **28**, 381 (1983).
[14] J. Sempau, E. Acosta, J. Baró, J. M. Fernández-Varea, and F. Salvat, Nucl. Instrum. Methods Phys. Res. B **132**, 377 (1997).
[15] E. Acosta, E. Coleoni, G. Castellano, J. A. Riveros, J. M. Fernández-Varea, and F. Salvat, Scanning Microsc. **10**, 625 (1996).
[16] OECD Nuclear Energy Agency Data Bank. Le Seine Saint-Germain, 12 Boulevard des Iles, 92130 Issy-les-Moulineaux, France (Electronic mail: NEA@db.nea.fr).
[17] J. Baró, J. Sempau, J. M. Fernńdez-Varea, and F. Salvat, Nucl. Instrum. Methods Phys. Res. B **100**, 31 (1995).
[18] R. Mayol and F. Salvat, At. Data Nucl. Data Tables **65**, 55 (1997).
[19] F. Salvat and J. M. Fernández-Varea, Nucl. Instrum. Methods Phys. Res. B **63**, 255 (1992).
[20] D. Lijequist, J. Phys. D **16**, 1567 (1983).
[21] M. J. Berger and S. M. Seltzer, National Bureau of Standards, Report NBSIR 82-2550 Washington D.C., 1982. Also available as ICRU Report No. 37, 1984.
[22] J. M. Fernández-Varea, R. Mayol, J. Baró, and F. Salvat, Nucl. Instrum. Methods Phys. Res. B **73**, 447 (1993).
[23] D. E. Cullen, M. H. Chen, J. H. Hubbell, S. T. Perkins, E. F. Plechaty, J. A. Rathkopf and J. H. Scofield, Lawrence Livermore National Laboratory, Report No. UCRL-50400, Vol. 6, Rev. 4, parts A and B, 1989.
[24] M. J. Berger and J. H. Hubbell, National Bureau of Standards, Report No. NBSIR 87-3797, Washington D.C. 1987.
[25] J. H. Hubbell, W. J. Veigele, E. A. Briggs, R. T. Brown, D. T. Cromer, and R. J. Howerton, J. Phys. Chem. Ref. Data **4**, 471 (1975); Erratum: *ibid.* **6**, 615 (1977).
[26] D. Brusa, G. Stutz, J. A. Riveros, J. M. Fernández-Varea, and F. Salvat, Nucl. Instrum. Methods Phys. Res. A **379**, 167 (1996).
[27] M. Inokuti, Rev. Mod. Phys. **43**, 297 (1971).
[28] R. Mayol and F. Salvat, J. Phys. B **23**, 2117 (1990).
[29] C. R. Worthington and S. G. Tomlin, Proc. Phys. Soc. London, Sect. A **69**, 401 (1956).
[30] X. Long, M. Lu, F. Ho, and X. Peng, At. Data Nucl. Data Tables **45**, 353 (1990).
[31] R. W. Fink and P. Venogulapa Rao, in *Handbook of Spectroscopy,* edited by J. W. Robinson (CRC, Cleveland, 1974), Vol. 1, p. 219.
[32] Md. R. Khan and M. Karimi, X-Ray Spectrom. **9**, 32 (1980).
[33] H. Bethe and W. Heitler, Proc. Phys. Soc. London, Sect. A **146**, 83 (1934).
[34] S. M. Seltzer and M. J. Berger, Nucl. Instrum. Methods Phys. Res. B **12**, 95 (1985).
[35] J. D. Jackson, *Classical Electrodynamics* (Wiley, New York, 1975), pp. 713–715.
[36] J. N. Chapman, C. C. Gray, B. W. Roberton, and W. A. P. Nicholson, X-Ray Spectrom. **12**, 153 (1983).
[37] K. Shima, Nucl. Instrum. Methods **165**, 21 (1979).

J. Appl. Phys., Vol. 83, No. 11, 1 June 1998

Acosta *et al.*   6049

[38] M. Krumrey, E. Tegeler, and G. Ulm, Rev. Sci. Instrum. **60**, 2287 (1989).

[39] D. L. Weathers, J. L. Duggan, M. R. McNeir, Y. C. Yu, F. D. McDaniel, C. A. Quarles, H. Lehtihet, and D. Kahler, Nucl. Instrum. Methods Phys. Res. B **56/57**, 964 (1991).

[40] S. J. B. Reed, *Electron Microprobe Analysis* (Cambridge University Press, Cambridge, 1993).

[41] M. C. Lépy, J. Plagnard, P. Stemmler, G. Ban, L. Beck, and P. Dhez, X-Ray Spectrom. **26**, 195 (1997).

[42] J. H. Paterson, J. N. Chapman, W. A. P. Nicholson, and J. M. Titchmarsh, J. Microsc. **154**, 1 (1989).

[43] P. J. Statham, J. Microsc. **123**, 1 (1981).

[44] E. Acosta, X. Llovet, E. Coleoni, F. Salvat and J. A. Riveros, X-Ray Spectrom. (in press).